Random Distributed Feedback Fiber Laser Generating Cylindrical Vector Beams

Jinghao Wang,[1] Ruishan Chen,[1] Junna Yao,[1] Hai Ming,[1] Anting Wang,[1,*] and Qiwen Zhan[2,3]

[1] *Department of Optics and Optical Engineering, University of Science and Technology of China, Hefei, 230026 Anhui, China*

[2] *Department of Electro-Optics and Photonics, University of Dayton, Dayton, Ohio 45469, USA*

[3] *School of Optical-Electrical and Computer Engineering, University of Shanghai for Science and Technology, 200093 Shanghai, China*

(Received 8 May 2018; revised manuscript received 4 February 2019; published 17 April 2019)

We experimentally demonstrate a random distributed feedback fiber laser generating cylindrical vector beams via a mode-selective coupler and a fiber ring resonator with 50-m-long single-mode fiber. Because of random distributed feedback provided by the single-mode fiber, multimode interactions are suppressed in the cavity, leading to modeless output. Azimuthally and radially polarized beams can both be obtained by adjustment of the polarization controllers. Speckle contrast measurements are made to confirm the effectiveness of the designed laser in reducing laser speckle. Apart from the low cost and simple technology of such a laser, the cylindrical vector beams with modeless behavior may have applications in areas such as laser radars, free-space communication, remote sensing, and biomedical imaging.

DOI: 10.1103/PhysRevApplied.11.044051

I. INTRODUCTION

Random lasers with optical feedback provided by multiple scattering compared with a well-defined cavity in conventional lasers have attracted a great deal of attention because of their low cost and special properties in the past few decades [1–7]. In traditional random lasers, laser output might suffer from problems such as complex emission spectra and angular dependence, making them less attractive in practical applications. To overcome these problems, low-dimensional random systems (e.g., random fiber lasers) were proposed to enhance the performance of random lasers [8–10]. One of the most-significant breakthroughs was made by Turitsyn *et al.* [10], who proposed a novel type of random fiber laser and named it a "random distributed feedback (DFB) fiber laser." In such a laser, the laser feedback is provided by Rayleigh backscattering resulting from refractive-index inhomogeneities of ultralong fibers. Different gains provided by stimulated Raman scattering [10], stimulated Brillouin scattering (SBS) [11] and active fibers [12] were used in random DFB fiber lasers to achieve operation in different spectral bands. Subsequently, the generation of multiple wavelengths [13], tunable wavelength [14], and a narrow spectrum [15] were realized in random DFB fiber lasers. Owing to their attractive features such as low cost, simple technology, and modeless behavior, random fiber lasers have potential applications in telecommunication, sensing, nonlinear optics, and imaging [16–19].

Cylindrical vector beams (CVBs), such as azimuthally and radially polarized beams, due to their special polarization and amplitude distributions [20], have shown great utility in the fields of high-resolution imaging [21], optical trapping [22], telecommunication [23], and sensing [24] in recent years. Because of their low cost, high efficiency, and good integration, all-fiber lasers have been successfully used to generate CVBs [25–28]. Until now there has been no report on a random DFB fiber laser generating CVBs. The combination of the special properties offered by CVBs and random fiber lasers would provide more potential applications for biomedical imaging, laser radars, free-space communication, and remote sensing. In the field of biomedical imaging, low-temporal-coherence sources are required in some technologies, such as optical coherence tomography [29], which has been widely applied in medical diagnosis and scientific research. A random fiber laser can achieve output with low temporal coherence, which is a useful option for optical coherence tomography. Resolution is one of the most-important performance parameters of an imaging system. A radially polarized beam has shown great advantages in high-resolution imaging since a tighter electric field spot can be obtained after tight focusing through a lens compared with the well-known linearly and circularly polarized beams [20,30,31]. The combined system is expected to be applied in optical coherence tomography to achieve high-resolution imaging. Besides, the low temporal coherence offered by random fiber lasers can be used to reduce laser speckle [32,33]. Low-temporal-coherence radially polarized beams are expected to be used in high-resolution biomedical imaging systems to

*atwang@ustc.edu.cn

provide better image quality. In practical application, some optical systems such as free-space optical communication, remote sensing and laser radar systems, will often suffer from turbulence-induced scintillation [34]. Both partially coherent beams and radially polarized beams have shown their effectiveness in reducing scintillation [35–38]. Recently, the scintillation index of a partially coherent radially polarized beam propagating through thermally induced turbulence was studied, showing that a partially coherent radially polarized beam has an advantage over a linearly polarized partially coherent beam in reducing turbulence-induced scintillation [38]. The combined system could be a high-integration miniaturization device in free-space optical communication, remote sensing, and laser radar systems. In addition, random fiber lasers are of low cost, which is attractive in the practical applications mentioned above.

In this paper, we propose and demonstrate a random fiber laser with CVB outputs. A mode-selective coupler (MSC) is inserted in the cavity as a mode converter to achieve mode conversion from the linearly polarized 01 (LP_{01}) mode to the linearly polarized 11 (LP_{11}) mode. The azimuthally and radially polarized beams are generated by our adjusting the polarization controllers (PCs) in the designed laser. A fiber ring resonator (FRR) is applied to provide random DFB. The light circulating in the FRR generates backscattered light through Rayleigh backscattering and SBS. Because of the random DFB, multimode interactions are suppressed in the cavity, leading to laser output with modeless and low coherence. The effectiveness of the designed laser in reducing laser speckle is confirmed by speckle contrast measurements. The proposed laser retaining the advantages of high integration and low cost offered by traditional optical fiber lasers while achieving low-coherence output can be used as a multifunctional laser source, which provides added value in many practical fields, such as laser radars, free-space communication, remote sensing, and biomedical imaging.

II. EXPERIMENTAL SETUP

Figure 1 shows a schematic diagram of the proposed fiber laser. A 1-m-long ytterbium-doped fiber (YDF) acting as a gain medium is pumped by a 980-nm laser diode through a 980-nm/1060-nm wavelength-division multiplexer. The YDF is followed by a FRR composed of a fiber coupler with a coupling ratio of 90:10 and a 50-m-long single-mode fiber (SMF) serving as one of the laser mirrors to provide random DFB. Unwanted Fresnel reflection at the output end of the fiber is eliminated by our inserting an isolator to ensure the random distributed scattering is the only feedback. A fiber loop mirror (FLM) made by a 3-dB coupler is used to form another laser mirror. The MSC is inserted between the FLM and the wavelength-division multiplexer for mode conversion and power output. PC1

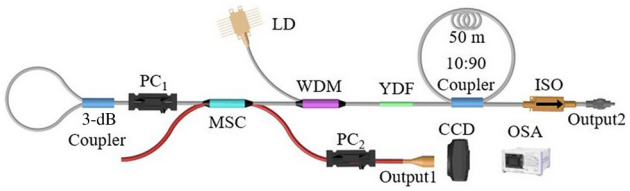

FIG. 1. The experimental setup of the proposed random DFB fiber laser generating CVBs. ISO, isolator; LD, laser diode; OSA, optical spectrum analyzer; PC_1, polarization controller 1; PC_2, polarization controller 2; WDM, wavelength-division multiplexer.

placed between the FLM and the MSC is used to control the polarization state of the fundamental mode. PC2 is used to refine the polarization of the output high-order mode. The laser output spectrum, power, and beam profile are measured by an optical spectrum analyzer with a resolution of 0.05 nm, a power meter and a CCD camera, respectively.

The MSC based on the modal coupling mechanism has been applied to generate CVBs successfully in previous studies [39–41]. A MSC is based on phase-matched evanescent coupling between two dissimilar fibers: a SMF and a few-mode fiber (FMF). According to coupled-mode theory [42], the ratio of the optical power of the two output ports of the MSC can be defined as α:

$$\alpha = \frac{P_2(l)}{P_1(l)} = \frac{K^2 \sin^2 \frac{Cl}{K}}{1 - K^2 \sin^2 \frac{Cl}{K}}, \tag{1}$$

where $K = [1 + (\beta_1 - \beta_2)^2/4C^2]^{-1/2}$, K^2 represents the maximum coupling power between two fibers, P_1 denotes the optical power of the LP_{01} mode in the SMF, P_2 denotes the optical power of the LP_{11} mode in the FMF, l is the length of the coupling region, C is mutual-coupling coefficient, and β_1 and β_2 represent the propagation constants of the LP_{01} and LP_{11} modes, respectively. When the phase-matching condition is satisfied and the loss is ignored, the mode-conversion efficiency γ from the LP_{01} mode at the input port of the SMF to the LP_{11} mode at the output port of the FMF can be written as

$$\gamma = \frac{P_2(l)}{P_1(l) + P_2(l)} = \sin^2 Cl. \tag{2}$$

According to Eq. (2), the mode-conversion efficiency is related to the length of the coupling region. During the fabrication process, the SMF and the FMF are twisted, fused, and stretched together to form a coupling region [43]. The output mode is confirmed by our observing output beam profiles through a CCD camera. The ratio of the output power of the SMF and the FMF is around 90:10 as measured by the power meter, indicating an output ratio of about 10% for the laser.

III. EXPERIMENTAL RESULTS AND DISCUSSION

Figures 2(a)–2(e) show the spectral characteristics of output 1 at different pump powers. When the pump power is below the lasing threshold of 75 mW, the output spectrum exhibits the behavior of amplified spontaneous emission, as shown in Fig. 2(a). When the pump power exceeds the threshold marginally, several spikes appear, as shown in Fig. 2(b). Figures 2(c)–2(e) show the measured spectra for pump powers of 120, 185, and 240 mW, respectively. Two parameters are proposed to quantitatively analyze the relationship between the spikes and the pump power; namely $\Delta\lambda$ and N, where $\Delta\lambda$ represents the spectral width for the spikes whose intensity is 10 dB lower than the maximal intensity of the spikes and N represents the number of spikes in the corresponding spectral width. Figure 2(f) shows the evolution of $\Delta\lambda$ and N versus the pump power.

The inset in Fig. 2(f) shows the frequency autocorrelation function of the lasing spectra. The horizontal axis of the inset shows the frequency shift, and the vertical axis stands for the normalized amplitude. The first peak, at around 14 GHz, corresponds to the separation of the lasing spikes at approximately 14 GHz (0.056 nm), which confirms that the spikes must be the Stokes lines of SBS. The light circulating counterclockwise in the FRR generates the backscattering light in the clockwise direction through Rayleigh scattering serving as the feedback into the cavity. The backscattering light is amplified as it passes through the YDF and couples back into the FRR. The light intensity in the FRR can be enhanced effectively due to coherent phase matching provided by the FRR. According to Ref. [44], the threshold of SBS in the FRR is given approximately by

$$P_{\mathrm{th}} = \frac{2A\pi}{gLF}, \tag{3}$$

where F is the finesse of the FRR, L is the length of the FRR, g is the Brillouin gain coefficient, and A is the effective core area. Using the parameters of the FRR applied in our experiment, we calculate the threshold of SBS in the FRR to be about 1.7 mW. The threshold input power of the FRR is even lower (approximately 0.18 mW) according to Eq. (6) in Ref. [44]. Since the threshold of SBS is quite low, the SBS process in the FRR can occur at low pump power. When the light intensity in the FRR reaches the threshold of SBS, the light is sent back by the SBS with high reflectivity [45]. With the increase of pump power, the power of lower-order SBS Stokes components is amplified enough to excite the higher-order SBS Stokes components in the FRR. Thus, more and more SBS Stokes components are generated in the laser cavity, leading to an increasing number of spikes in the output spectra.

The laser power at output 1 and output 2 versus pump power is shown in Fig. 3. When the pump power is below the threshold of 75 mW, the output power is close to 0 mW, but increases linearly with the pump power after the pump power exceeds 75 mW, presenting the same threshold behavior, which confirms the spectral analysis above. According to the red curve in Fig. 3, the slope efficiency

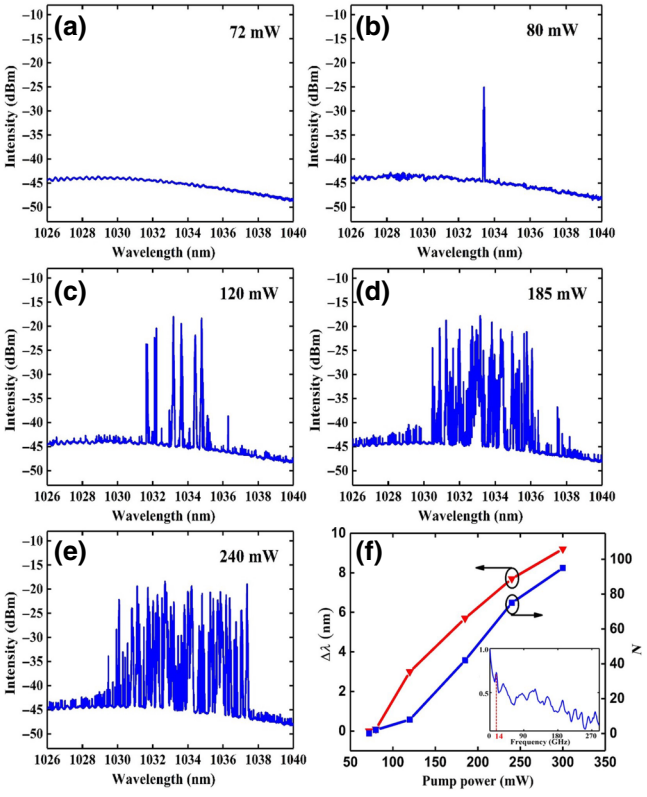

FIG. 2. Laser spectra at different pump powers of (a) 72 mW, (b) 80 mW, (c) 120 mW, (d) 185 mW, and (e) 240 mW. (f) The evolution of $\Delta\lambda$ and N versus the pump power. The inset shows the frequency autocorrelation function of the lasing spectra at a pump power of 240 mW.

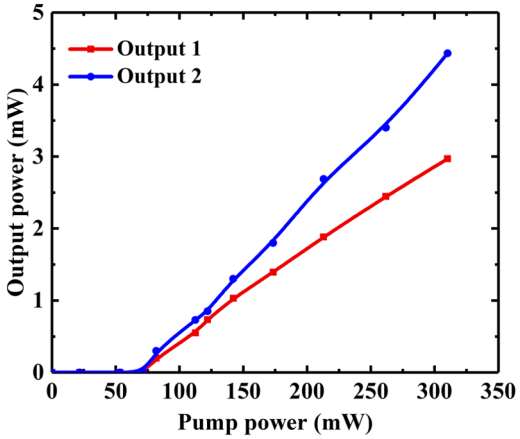

FIG. 3. Laser output power versus pump power.

of CVBs at output port 1 is about 1.2%. The slope efficiency at output port 2 is about 2.1%, as shown in Fig. 3 by the blue curve. The total slope efficiency is calculated to be 3.3%. By adjusting the intracavity PCs, we can obtain azimuthally and radially polarized beams with doughnut-shaped intensity profiles as shown in Figs. 4(a) and 4(f), respectively. PC1 is used to control the polarization of the fundamental mode in the cavity. PC2 in the few-mode fiber is used to refine the polarization of the output higher-order mode such that the TE_{01} and TM_{01} modes can be selected [25–28,40,41]. By our rotating a linear polarizer inserted between the collimator and the CCD, the polarization states of output beams can be confirmed. Figures 4(b)–4(e) show the intensity profiles of the beam after the azimuthally polarized beam has passed through the linear polarizer at four transmission axes (denoted by the white arrows). Figures 4(g)–4(j) show the intensity profiles of the beams after the radially polarized beam has passed through the linear polarizer. By using the fiber bending method proposed in Ref. [25], we measure the mode purities of the azimuthally and radially polarized beams to be about 95% and 94.5%, respectively.

In imaging, laser speckle is one of the important factors affecting imaging quality. There are various ways to reduce speckle, including applying low-coherence sources. CVBs, because of their special polarization distributions, have low spatial coherence compared with ordinary linearly polarized beams, so CVBs can be used to reduce laser speckle. Since the cylindrical vector modes (namely, the TE_{01} mode and the TM_{01} mode) have an axial-symmetry polarization distribution, they can be decomposed into two orthogonal linearly polarized modes [30]. The application of orthogonal linearly polarized beams has shown its advantage in decreasing speckle contrast compared with use of a linearly polarized beam alone [32]. To confirm the effectiveness of the designed laser in reducing laser speckle, speckle contrast measurements are performed. Plots (a)-(c) in the top row in Fig. 5 show the intensity distributions of the single-wavelength linearly polarized beam, the single-wavelength radially polarized beam, and the multiwavelength radially polarized beam generated by the designed random DFB fiber laser. The emission spectra are shown in the second row in Fig. 5. The third row in Fig. 5 shows the speckle patterns of the corresponding beams passing through the diffuser, where the corresponding speckle contrasts are also marked. We can see that speckle contrast decreases by about 21% when the single-wavelength radially polarized beam is used compared with when the single-wavelength linearly polarized beam is used. The use of the multiwavelength radially polarized beam reduces the speckle contrast by a further 16% compared with the use of the single-wavelength radially polarized beam. The results show that the designed

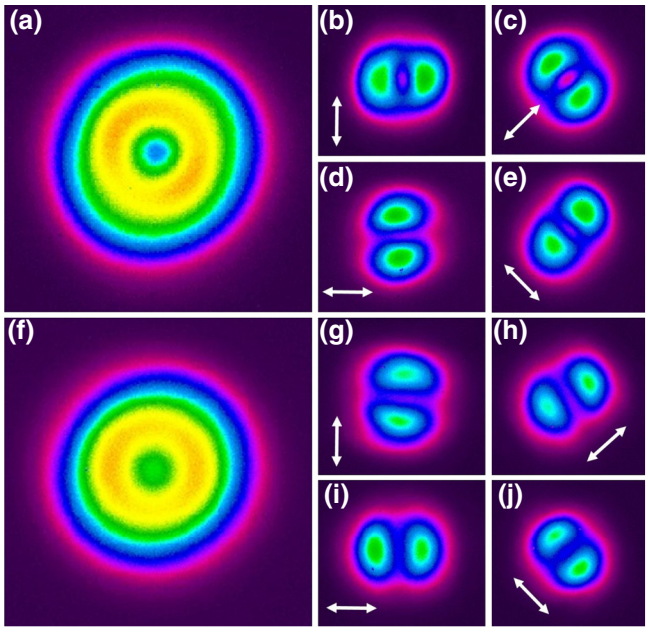

FIG. 4. (a) Intensity profiles of the azimuthally polarized beam and (b)–(e) the corresponding evolution after the beam has passed through a linear polarizer with four orientations denoted by the white arrows. (f) Intensity profiles of the radially polarized beam and (g)–(j) the corresponding evolution after the beam has passed through the linear polarizer.

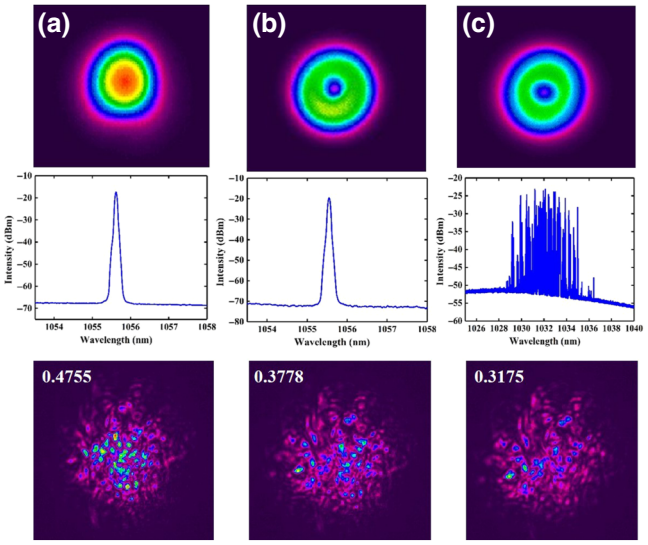

FIG. 5. The top row shows the intensity distributions of (a) the single-wavelength linearly polarized beam, (b) the single-wavelength radially polarized beam, and (c) the multiwavelength radially polarized beam generated by the designed random DFB fiber laser. The second row shows the emission spectra of the corresponding beams. The third row shows the speckle patterns of the corresponding beams passing through the diffuser, where corresponding speckle contrasts are marked in the upper-left corner of the speckle patterns.

laser can be used to reduce the influence of laser speckle, which is useful in many imaging systems.

IV. CONCLUSIONS

In summary, a random DFB fiber laser generating CVBs is successfully demonstrated. Owing to random DFB provided by the FRR with a 50-m-long SMF, the laser achieves CVBs with modeless behavior. The increase in the number of spikes in the output spectrum with increasing pump power is attributed to the cascaded SBS mechanism. The relatively low efficiency of the designed laser is attributed to the insertion of the MSC, and the efficiency could be enhanced greatly by improvement of the technique for fabrication of the MSC. High-purity azimuthally and radially polarized beams are produced by our controlling the polarization states in the fiber cavity. Speckle contrast measurements show the effectiveness of the designed laser in reducing laser speckle. The designed laser has typical characteristics of random fiber lasers, such as low cost, high integration, and output with low coherence but high intensity, which may have applications in laser radars, free-space communication, remote sensing, and biomedical imaging.

ACKNOWLEDGMENTS

This work was supported by the National Natural Science Foundation of China (Grant No. 61275049).

J.W. and R.C contributed equally to this work.

[1] V. Letokhov, Generation of light by a scattering medium with negative resonance absorption, Sov. J. Exp. Theor. Phys. **26**, 835 (1968).

[2] M. P. VanAlbada and A. Lagendijk, Observation of Weak Localization of Light in a Random Medium, Phys. Rev. Lett. **55**, 2692 (1985).

[3] H. Cao, Lasing in random media, Waves Random Media **13**, R1 (2003).

[4] S. Gottardo, R. Sapienza, P. D. García, A. Blanco, D. S. Wiersma, and C. López, Resonance-driven random lasing, Nat. Photonics **2**, 429 (2008).

[5] D. S. Wiersma, The physics and applications of random lasers, Nat. Phys. **4**, 359 (2008).

[6] N. M. Lawandy, R. Balachandran, A. Gomes, and E. Sauvain, Laser action in strongly scattering media, Nature **368**, 436 (1994).

[7] H. Cao, Y. G. Zhao, S. T. Ho, E. W. Seelig, Q. H. Wang, and R. P. H. Chang, Random Laser Action in Semiconductor Powder, Phys. Rev. Lett. **82**, 2278 (1999).

[8] C. J. de Matos, L. D. S. Menezes, A. M. Brito-Silva, M. M. Gámez, A. S. Gomes, and C. B. de Araújo, Random Fiber Laser, Phys. Rev. Lett. **99**, 153903 (2007).

[9] Z. Hu, Q. Zhang, B. Miao, Q. Fu, G. Zou, Y. Chen, Y. Luo, D. Zhang, P. Wang, H. Ming, and Q. Zhang, Coherent Random Fiber Laser Based on Nanoparticles Scattering in the Extremely Weakly Scattering Regime, Phys. Rev. Lett. **109**, 253901 (2012).

[10] S. K. Turitsyn, S. A. Babin, A. E. El-Taher, P. Harper, D. V. Churkin, S. I. Kablukov, J. D. Ania-Castañón, V. Karalekas, and E. V. Podivilov, Random distributed feedback fibre laser, Nat. Photonics **4**, 231 (2010).

[11] M. Pang, S. Xie, X. Bao, D.-P. Zhou, Y. Lu, and L. Chen, Rayleigh scattering-assisted narrow linewidth Brillouin lasing in cascaded fiber, Opt. Lett. **37**, 3129 (2012).

[12] M. Fan, Z. Zon, X. Tian, D. Xu, D. Zhou, R. Zhang, N. Zhu, L. Xie, H. Li, J. Su, and Q. Zhu, Comprehensive investigations on 1053 nm random distributed feedback fiber laser, IEEE Photonics J. **9**, 1 (2017).

[13] S. Sugavanam, Z. Yan, V. Kamynin, A. Kurkov, L. Zhang, and D. Churkin, Multiwavelength generation in a random distributed feedback fiber laser using an all fiber Lyot filter, Opt. Express **22**, 2839 (2014).

[14] S. A. Babin, A. E. El-Taher, P. Harper, E. V. Podivilov, and S. K. Turitsyn, Tunable random fiber laser, Phys. Rev. A **84**, 021805 (2011).

[15] S. Sugavanam, N. Tarasov, X. Shu, and D. V. Churkin, Narrow-band generation in random distributed feedback fiber laser, Opt. Express **21**, 16466 (2013).

[16] S. A. Babin, E. Dontsova, and S. Kablukov, Random fiber laser directly pumped by a high-power laser diode, Opt. Lett. **38**, 3301 (2013).

[17] Z. Wang, Y. Rao, H. Wu, P. Li, Y. Jiang, X. Jia, and W. Zhang, Long-distance fiber-optic point-sensing systems based on random fiber lasers, Opt. Express **20**, 17695 (2012).

[18] A. A. Fotiadi, Random lasers: An incoherent fibre laser, Nat. Photonics **4**, 204 (2010).

[19] B. Redding, M. A. Choma, and H. Cao, Speckle-free laser imaging using random laser illumination, Nat. Photonics **6**, 355 (2012).

[20] R. Dorn, S. Quabis, and G. Leuchs, Sharper Focus for a Radially Polarized Light Beam, Phys. Rev. Lett. **91**, 233901 (2003).

[21] Y. Xue, C. Kuang, S. Li, Z. Gu, and X. Liu, Sharper fluorescent super-resolution spot generated by azimuthally polarized beam in STED microscopy, Opt. Express **20**, 17653 (2012).

[22] T. Kuga, Y. Torii, N. Shiokawa, T. Hirano, Y. Shimizu, and H. Sasada, Novel Optical Trap of Atoms with a Doughnut Beam, Phys. Rev. Lett. **78**, 4713 (1997).

[23] Y. Zhao and J. Wang, High-base vector beam encoding/decoding for visible-light communications, Opt. Lett. **40**, 4843 (2015).

[24] Y. Cai, Q. Lin, H. T. Eyyuboğlu, and Y. Baykal, Average irradiance and polarization properties of a radially or azimuthally polarized beam in a turbulent atmosphere, Opt. Express **16**, 7665 (2008).

[25] B. Sun, A. Wang, L. Xu, C. Gu, Z. Lin, H. Ming, and Q. Zhan, Low-threshold single-wavelength all-fiber laser generating cylindrical vector beams using a few-mode fiber Bragg grating, Opt. Lett. **37**, 464 (2012).

[26] B. Sun, A. Wang, C. Gu, G. Chen, L. Xu, D. Chung, and Q. Zhan, Mode-locked all-fiber laser producing radially polarized rectangular pulses, Opt. Lett. **40**, 1691 (2015).

[27] Y. Zhou, K. Yan, R. Chen, C. Gu, L. Xu, A. Wang, and Q. Zhan, Resonance Efficiency Enhancement for Cylindrical Vector Fiber Laser with Optically Induced Long Period Grating, Appl. Phys. Lett. **110**, 161104 (2017).

[28] R. Chen, J. Wang, X. Zhang, A. Wang, H. Ming, F. Li, D. Chung, and Q. Zhan, High efficiency all-fiber cylindrical vector beam laser using a long-period fiber grating, Opt. Lett. **43**, 755 (2018).

[29] D. Huang, E. A. Swanson, C. P. Lin, J. S. Schuman, W. G. Stinson, W. Chang, M. R. Hee, T. Flotte, K. Gregory, C. A. Puliafito, and J. G. Fujimoto, Optical coherence tomography, Science **254**, 1178 (1991).

[30] Q. Zhan, Cylindrical vector beams: From mathematical concepts to applications, Adv. Opt. Photonics **1**, 1 (2009).

[31] G. M. Lerman and U. Levy, Effect of radial polarization and apodization on spot size under tight focusing conditions, Opt. Express **16**, 4567 (2008).

[32] J. W. Goodman, *Speckle phenomena in optics* (Roberts & Co., Greenwood Village, CO, 2007).

[33] S. Shin, K. Kim, K. Lee, S. Lee, and Y. Park, Effects of spatiotemporal coherence on interferometric microscopy, Opt. Express **25**, 8085 (2017).

[34] L. Andrews, R. Phillips, and C. Hopen, *Laser beam scintillation with applications* (SPIE, Bellingham, WA, 2001), Vol. 99.

[35] O. Korotkova, Scintillation index of a stochastic electromagnetic beam propagating in random media, Opt. Commun. **281**, 2342 (2008).

[36] S. Wang, Y. Baykal, and M. Plonus, Receiver-aperture averaging effects for the intensity fluctuation of a beam wave in the turbulent atmosphere, JOSA **73**, 831 (1983).

[37] W. Cheng, J. W. Haus, and Q. Zhan, Propagation of vector vortex beams through a turbulent atmosphere, Opt. Express **17**, 17829 (2009).

[38] F. Wang, X. Liu, L. Liu, Y. Yuan, and Y. Cai, Experimental Study of the Scintillation Index of a Radially Polarized Beam with Controllable Spatial Coherence, Appl. Phys. Lett. **103**, 091102 (2013).

[39] H. Wan, J. Wang, Z. Zhang, Y. Cai, B. Sun, and L. Zhang, High efficiency mode-locked, cylindrical vector beam fiber laser based on a mode selective coupler, Opt. Express **25**, 11444 (2017).

[40] T. Wang, F. Wang, F. Shi, F. Pang, S. Huang, T. Wang, and X. Zeng, Generation of femtosecond optical vortex beams in all-fiber mode-locked fiber laser using mode selective coupler, J. Lightwave. Technol. **35**, 2161 (2017).

[41] R. Ismaeel, T. Lee, B. Oduro, Y. Jung, and G. Brambilla, All-fiber fused directional coupler for highly efficient spatial mode conversion, Opt. Express **22**, 11610 (2014).

[42] W.-P. Huang, Coupled-mode theory for optical waveguides: An overview, JOSA A **11**, 963 (1994).

[43] F. Wang, F. Shi, T. Wang, F. Pang, T. Wang, and X. Zeng, Method of generating femtosecond cylindrical vector beams using broadband mode converter, IEEE Photonics. Technol. Lett. **29**, 747 (2017).

[44] R. Kadiwar, P. Bayvel, and I. Giles, in *Fiber Optic and Laser Sensors VI* (International Society for Optics and Photonics, 1989), Vol. 985, p. 338–344.

[45] Z. Pan, L. Meng, Q. Ye, H. Cai, Z. Fang, and R. Qu, Repetition rate stabilization of the SBS Q-switched fiber laser by external injection, Opt. Express **17**, 3124 (2009).